Sustainable High Capacitance at High Frequencies: Metallic Aluminum–Polypropylene Nanocomposites

Lisa A. Fredin,[†] Zhong Li,[†] Michael T. Lanagan,[‡,*] Mark A. Ratner,[†,*] and Tobin J. Marks[†,*]

[†]Department of Chemistry and the Materials Research Center, Northwestern University, Evanston, Illinois 60208-3113, United States and [‡]Department of Engineering Science and Mechanics, Materials Research Institute, The Pennsylvania State University, University Park, Pennsylvania 16802-4800, United States

ABSTRACT The high-frequency dielectric response of 0–3 polypropylene nanocomposites prepared with the activated metallocene polymerization catalyst [*rac*-ethylenebisindenyl]zirconium dichlororide absorbed on the native Al_2O_3 surfaces of metallic aluminum nanoparticles is characterized. The nanocomposites produced are randomly dispersed in the polyolefin matrix with no visible defects that might degrade film dielectric properties. Electrical measurements show that as the volume fraction of Al nanoparticles is increased, the effective permittivity of the nanocomposites increases, with ε_r values reaching ~10 at relatively low frequency (1 MHz). Because of the high permittivity and conductivity contrast between the metal nanoparticles and the polypropylene matrix, Maxwell–Wagner–Sillars theory can be applied to model the loss at high frequencies and provide insight into how the nanocomposite high frequency response scales with Al volume fraction. At higher Al nanoparticle volume fractions, mixing theories predict greater densities of nanoparticle aggregates, consistent with the experimentally observed shift of the dielectric relaxation to lower frequencies. Although these nanocomposites undergo the predicted initial dielectric relaxation with increasing frequency, the metallic nanoparticle complex permittivity imbues the higher Al volume fraction materials with relatively high, sustainable permittivities, 6, at frequencies as high as 7 GHz.

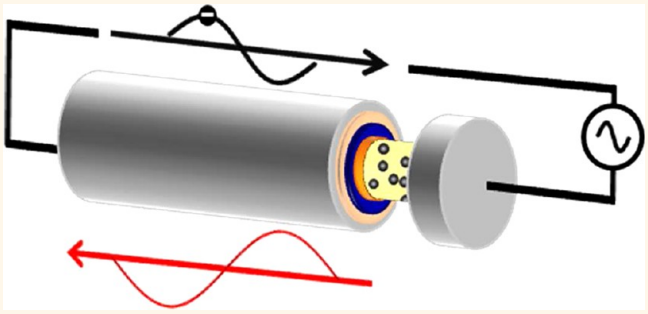

KEYWORDS: nanocomposite · metallic nanoparticle · dielectric materials · dielectric loss · frequency response · metal–insulator structures · inhomogeneous media

Metal particle dielectrics have very high permittivities, with ε_r values theoretically approaching infinity at low working voltages; however, such materials are difficult to process into multilayer thin films without high temperature sintering.[1,2] In contrast, the low dielectric permittivities of polymer dielectrics limit their applications, despite the good dielectric strength and facile processability.[3,4] Inorganic–polymer nanocomposite materials have recently received intensive study since they can combine the best properties of both phases, yielding potential collective performance well beyond that of each individual constituent material.[5–9] Thus, ceramic oxide particles with high permittivities (ranging from 50 to thousands) have been mechanically dispersed in polymer matrices to yield 0–3 composites (this notation indicates a zero-dimensional structure, *e.g.*, spheres, in a three-dimensional matrix) which are both processable and exhibit impressive permittivities well above that of the surrounding matrix[10,11] and moderate stored energies up to ~10 J/cm^3.[12–16] These observations then raise the intriguing question of what properties analogous systems containing metallic nanoparticles might exhibit. Owing to their expected higher *k* values metal–polymer composites might provide far higher capacitance than their ceramic counterparts. This promise has increased interest in metal–polymer composites over other conductive material-polymer solutions because of the ease of processing. Researchers have investigated various materials, such as, silver and gold-epoxy composites[11,17–21] mostly with small particles <10 nm in diameter or larger conductive particles–ferroelectric polymer blends[2,22,23] for higher permittivies at low frequencies; however, these composites often have high losses ($\tan\delta > 0.3$).[19,20,22,23]

* Address correspondence to mxl46@psu.edu, ratner@chem.northwestern.edu, t-marks@northwestern.edu.

Received for review September 24, 2012 and accepted December 13, 2012.

Published online December 24, 2012
10.1021/nn3044148

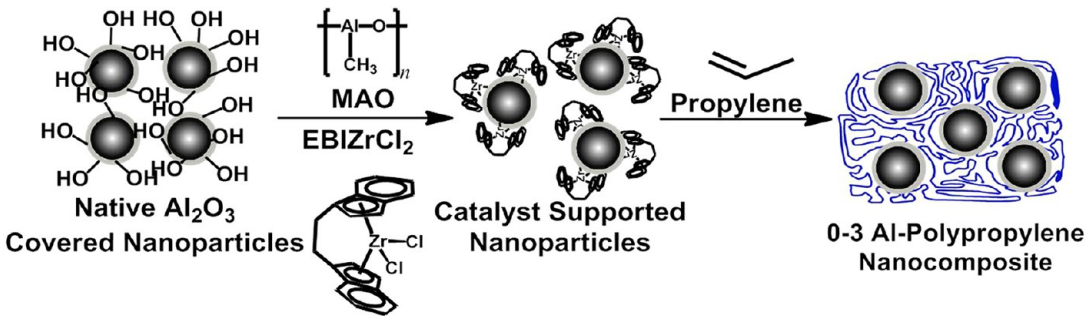

Scheme 1. Representation of Al nanoparticle−polypropylene composite synthesis

While these composites show promise with extremely high−permittivities greater than hundreds−they are limited by their preparation *via* conventional mixing methods and have not been extensively studied at higher frequencies.

This contribution focuses on the high frequency dielectric properties of metal−polyolefin nanocomposites prepared *via* the *in situ* polymerization of propylene by an organometallic polymerization catalyst adsorbed on the native oxide surfaces of metallic aluminum nanoparticles (see below). Previously, metallocene olefin polymerization catalysts supported[24−27] on oxide nanoparticles were employed to prepare, *in situ,* extensive series of 0−3 composites with $BaTiO_3$, TiO_2, ZrO_2, yttria-stabilized ZrO_2, $SrTiO_3$, $Ba_{0.5}Sr_{0.5}TiO_3$, and MgO nanoparticle fillers dispersed in polyolefin matrices (polypropylene, polyethylene, polystyrene, and other olefin copolymers).[16,28,29] The composites fabricated using this *in situ* approach exhibit moderate permittivities and low dielectric loss with little frequency dependence below 1 MHz, thus promising high recoverable energy storage (up to ∼10 J/cm^3), and graceful breakdown characteristics.[16,28,30,31] Note however that at frequencies above 1 MHz, these nanocomposites undergo deleterious dielectric relaxation which significantly degrades the capacitance.[16,28] The resulting low permittivities are therefore unsuitable for high-frequency applications (*e.g.*, GHz). Indeed, most materials development in the field has instead focused on thin-film ferroelectrics or liquid crystalline materials.[32−35] Importantly, improved dielectric materials with high capacitance and frequency-insensitive response to electromagnetic fields ranging from radio frequency through THz are essential for next-generation electronic products such as coaxial resonators, dielectric resonator filters, and substrates, particularly for frequencies in the 1−5 GHz range.[32,36]

Recently, the aforementioned *in situ* synthetic approach was applied to *metallic* aluminum nanoparticles having a 2 nm native oxide coating (Scheme 1).[31] It was found that the complex permittivity of the metallic Al particles affords composites with high permittivities, up to ∼15 at 100 Hz, and significant recoverable energy storage, ∼14 J/cm^3. Notably, these composites maintain permittivities greater than 10 up to 1 MHz, with only the highest Al volume fraction (0.12) material exhibiting significant relaxation in the 100 Hz to 1 MHz range.[16] These observations raise the question of whether the complex permittivity of metal nanoparticles can support sustainable high permittivities, > 4 in polymer nanocomposites above 1 GHz.[37]

Thin film capacitors are used in diverse high frequency electronic applications ranging from signal coupling, filtering, and impedance matching to advanced packaging applications.[38] The scalable production and facile processability of polyolefin nanocomposite thin films offers a potential replacement for ceramic thin films in real-world applications. Such thin films could have intrinsically lower inductances than multilayer ceramic capacitors because of the high mutual inductance between the internal counter electrodes in the multilayers. It is also expected that thin films would facilitate reductions in electronic system size and other improvements in performance for high-frequency circuitry.[38]

With regard to characterizing the present materials, the frequency dependence of permittivities is conventionally measured using dielectric relaxation spectroscopy (DRS) which probes the interaction of the sample with a time-dependent electric field.[39] The resulting polarization, expressed by the frequency-dependent complex permittivity (here by the real permittivity and tan δ), characterizes the amplitude and time scale of charge density fluctuations across the sample. Such fluctuations generally arise from electronic polarization, or more significantly, the reorientation of permanent molecular dipole moments, of nanoparticles or of dipolar moieties appended to polymers.[40] Other possible mechanisms include ion transport or the reorganization of interfacial charge in heterogeneous systems,[41−43] with the time scale of the fluctuations depending on the material and the relevant relaxation mechanism. Relaxation time scales range from psec in low-viscosity liquids to hours in glasses,[43] with the corresponding frequencies encompassing 0.1 mHz to 1 THz, (Figure 1).

Since in all polarization mechanisms (except those at optical frequencies arising from electronic polarization)

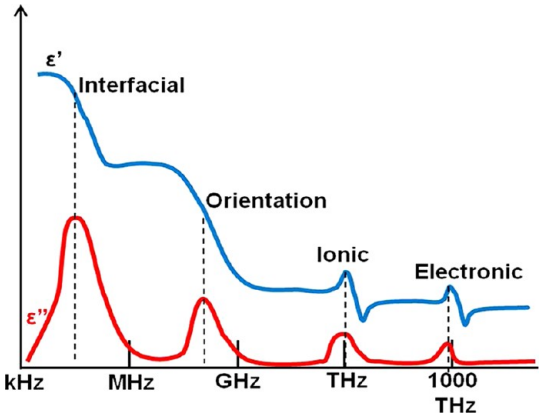

Figure 1. Real (ε') and imaginary (ε'') parts of the complex permittivity for a material having interfacial, orientational, ionic, and electronic polarization. The frequencies shown are typical of homogeneous materials reported in the literature, with the type of relaxation and approximate characteristic frequency indicated.

the dipolar response to an oscillating field involves displacement of masses, inertia constrains arbitrarily rapid movements. Two physical parameters describe the movement of the charged masses in response to alternating fields, polarization response and relaxation. Response can be modeled kinematically and relaxation describes the decay of polarization from excited states to the ground state.[41,44] As noted above, each response type has a characteristic relaxation frequency as shown in Figure 1. Maxwell–Wagner–Sillars (MWS) polarization is the interfacial polarization between the internal dielectric boundary layers in a material,[39] and generally occurs between the (slower) macroscopic interfacial relaxation at the electrode-dielectric layer interface and the (faster) orientational relaxation in the GHz range. While both MWS polarization and macroscopic interfacial polarization are due to the reorganization of charges at surfaces, MWS polarization contributes orders of magnitude less to the permittivity than does the electrode interface polarization due to the microscopic nature of the internal dielectric surfaces. However, MWS also exhibits polarization response until much higher frequencies because there are far fewer charges that must reorganize in the oscillating field, resulting in lower reorganization energies and potential faster reorganization times.

Here we analyze the frequency response of the aforementioned Al–polypropylene nanocomposites between 200 MHz and 7 GHz to understand the types of dielectric relaxation operative in the present metallic nanocomposites. From MWS modeling, it is argued that conductive particle aggregation leads to strong dielectric relaxation, where increasing aggregate size depresses the relaxation frequencies. Mixing approaches such as percolation theory, which accurately predict permittivities for typical nanocomposites at low frequencies,[31] argue that higher volume fractions of extremely high permittivity nanoparticles ($\varepsilon_r > 2000$)[16]

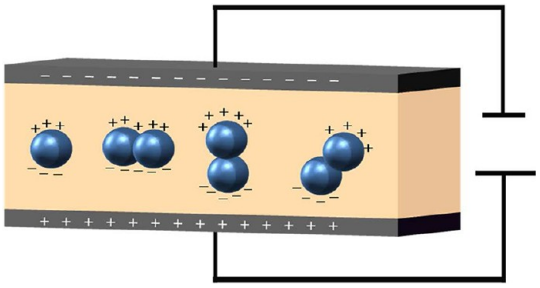

Figure 2. Applied voltage induces charges on each of the electrodes. The corresponding polarization of the nanoparticles within the matrix results in charge accumulation at the particle surface. The response of these charges to the oscillating field is the MWS polarization. Shown here are possible orientations of an aligned two-particle aggregate compared to a single isolate particle.

lead to aggregates (*e.g.*, chains) of particles that behave like single particles (at least for transport). For ferroelectric materials, such particle chains are thought to exhibit a combined dipole moment which responds to the field, resulting in dipolar polarization.[6,16,17,28,45] In contrast, conductive particle surfaces instead accumulate charge at interfaces with the matrix, which effectively thin the dielectric layer and cause additional interfacial MWS polarization (Figure 2).[39] These internal interfacial polarizations can be a major component of the dielectric response of the material and are highly sensitive to the orientation and alignment of the charge accumulation surfaces. MWS modeling offers a means to quantify the loss and frequency dependence of this polarization using geometrical arguments based on the conductive particle shape and orientation. Here we show that above ~0.10 volume fraction, Al–polypropylene nanocomposites have relatively high permittivities that are sustainable up to at least 5 GHz, and that composites with high Al volume fractions undergo relaxation at lower frequencies than their lower volume fraction counterparts.

RESULTS AND DISCUSSION

Nanocomposite Synthesis. Metal nanoparticle–polyolefin composites were prepared by chemisorbing a metallocene precatalyst, [*rac*-ethylenebisindenyl]zirconium dichloride (EBIZrCl$_2$) onto the native oxide of Al nanoparticles.[31] Addition of a methylaluminoxane (MAO) cocatalyst then activates the adsorbed EBIZrCl$_2$ for *in situ* synthesis of isotatic polypropylene (Scheme 1). Capacitors were then fabricated with films of these materials for dielectric characterization (see Methods for details and Figure 3 for characterization of film properties). As seen in other ceramic composites fabricated using this *in situ* polymerization method, the present composite films have no discernible voids[16,28] and the transmission electron microscopy (TEM) and scanning electron microscopy (SEM) images of the films indicate reasonably uniform morphologies (Figure 3). The native Al_2O_3 coating on the particles is ~2 nm thick

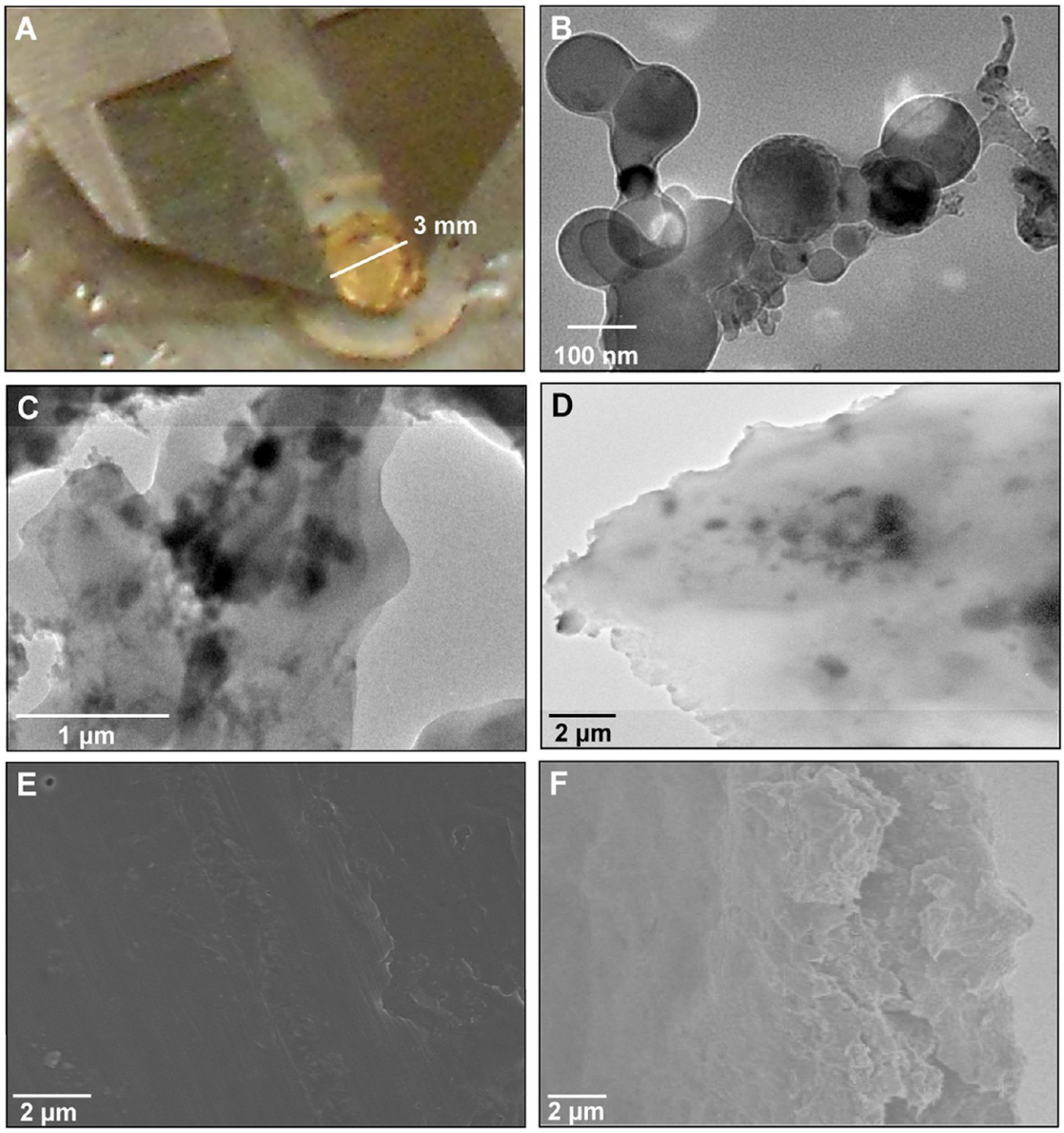

Figure 3. (A) Photograph of a thick film prepared in a PET washer, and TEM image of (B) Al nanoparticles after washing, (C) as fabricated composite powder, and (D) melt-processed composite powder of the 0.104 v_f composite where the dark spots are nanoparticles; as well as, SEM characterization of a 0.104 v_f composite (E) thick film surface and (F) thin film torn edge.

as confirmed by TEM. Note that this oxide thickness is comparable to that of a single Al_2O_3 layer derived from exposing methylaluminoxide (MAO) to air as used in our previous studies of ceramic nanoparticle–polyolefin composites,[16,28,46] and is thin enough that the volume fraction of Al metal in the samples is equivalent to the volume fraction of nanofiller.

Nanocomposite High Frequency Permittivity. The complex reflection (both magnitude, Γ, and phase, θ) for these nanocomposite capacitors was measured using lumped impedance methods.[47−50] From the magnitude and phase of the complex reflection, the dielectric permittivities, eq 1, of the thick films can be calculated. Here ω is the radial frequency, $C_o = A_{\varepsilon o}/d$, A is the area, d is the thickness of the sample, and Z_o is the characteristic impedance of a lossless transmission line (50 Ω).

$$\varepsilon_r' = \frac{2\Gamma \sin\theta}{\omega C_o Z_o(\Gamma^2 + 2\Gamma\cos\theta + 1)} \quad (1)$$

Figure 4 summarizes the frequency-dependent permittivity of Al-^{iso}PP nanocomposites as a function of composition from 200 MHz to 7 GHz. For the lowest volume fraction Al nanocomposites (0.007−0.029), the high frequency permittivities are statistically indistinguishable and ∼2. This is consistent both with the low measured permittivities at lower frequencies and the fact that these samples have very little MWS polarization but instead are expected to have dielectric relaxation dominated by optical relaxations which occur at

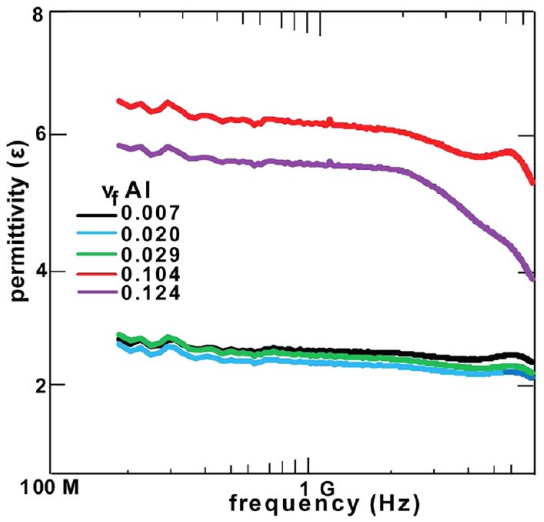

Figure 4. Permittivity of Al-*iso*PP nanocomposites from 100 MHz to 7 GHz as a function of Al nanoparticle volume fraction. Note: the 0.124 Al-composite has already undergone a permittivity relaxation before 1 MHz.[31].

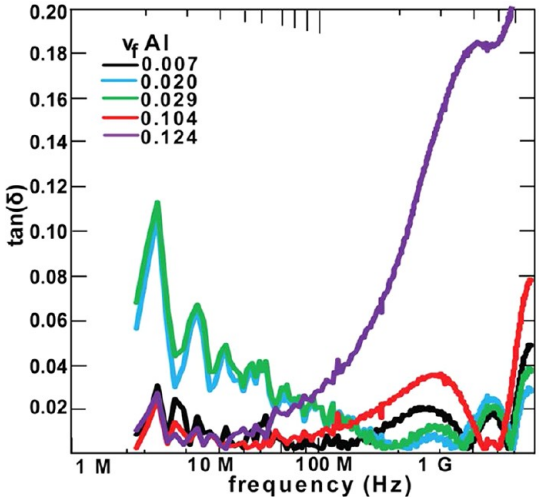

Figure 5. Graph showing tan δ of Al-*iso*PP nanocomposites as a function of nanoparticle volume fraction from 100 MHz to 7 GHz.

frequencies higher than 7 GHz.[39,51] The 0.104 volume fraction composite has a permittivity ~10 at 1 MHz but experiences a relaxation between 1 and 200 MHz, and the dielectric permittivity falls to ~6 by 200 MHz, and falls further as 7 GHz is approached. The permittivity of the 0.124 composite begins to undergo a dielectric relaxation before 1 M decreases by ~50% between 1 and 200 MHz and appears to have another relaxation near 5 GHz. Nevertheless, it maintains a permittivity >5 at frequencies between 200 MHz and 5 GHz. The observed relaxations in the hundreds of MHz are most likely a result of MWS interfacial relaxations (see more below) while the relaxations in the GHz range may also be orientational polarization relaxations from the polymer matrix.[41,42] In polymer films, typical orientational relaxations arise from dipolar groups attached to the backbone and small oscillations of the chain geometries, especially reorientation of chain ends.[40]

It will be seen that while the 0.104 and 0.124 volume fraction Al nanocomposites undergo a dielectric relaxation and permittivity decrease of almost 50% between 1 and 200 MHz, they maintain relatively large permittivities (~6) in the 200 MHz to 7 GHz range. Note that these materials appear to undergo another relaxation around 5−7 GHz. Relatively frequency-insensitive, high permittivities in the GHz range make these composites ideal candidates for high frequency dielectric applications.[52] The ceramic particle counterparts to these composites all have permittivities below 2 by 100 MHz and common radio frequency dielectrics have permittivities on the order of 3−4.[37]

Nanocomposite High Frequency Dielectric Loss. The value of tan δ is the imaginary part divided by the real part of the permittivity (tan $\delta = \varepsilon''/\varepsilon'$).

$$\varepsilon_r'' = \frac{1 - \Gamma^2}{\omega C_o Z_o(\Gamma^2 + 2\,\Gamma\cos\theta + 1)} \qquad (2)$$

By calculating both the real part (eq 1) and the imaginary part (eq 2) of the permittivity from the measured complex reflection, tan δ is obtained (Figure 5). Because the present lumped impedance technique measures the permittivity *via* a reflection method, there is some noise in the derived imaginary part of the permittivity, which introduces tan δ noise due to the very high measured magnitude of the reflection, Γ. The loss, tan δ, is proportional to the difference between the reflection magnitude of the sample and perfect reflection (100%). Lumped impedance measurements are typically limited to higher loss systems;[53] however, since the measured tan δ here is greater than 0.02, this should not be a major concern. However, overall these composites have relatively low loss, since up to 7 GHz the loss remains below 0.20.

As expected from the trends in permittivity, the tan δ of the 0.124 volume fraction Al nanocomposite begins to rise dramatically around 1 GHz, resulting in the permittivity fall evident in Figure 4. For both the 0.104 and 0.124 volume fraction materials, the permittivity data suggest a dielectric relaxation in the MHz range, but since the accuracy of the tan δ data in this region does not allow extraction of the exact frequency of this relaxation, the maximum in tan δ is not well-determined. Such GHz frequency relaxations seen in the high volume fraction polymer composites are most often attributed to orientational relaxation such as rotation of dipolar groups around bonds, chain twisting, or libration.[54] In ordered polymers lacking dipolar groups as in isotatic polypropylene, such polarizations have been assigned to chain end rotation,[40] and therefore this relaxation is a fairly small fraction of the total response. Because the polypropylene is grown *in situ*

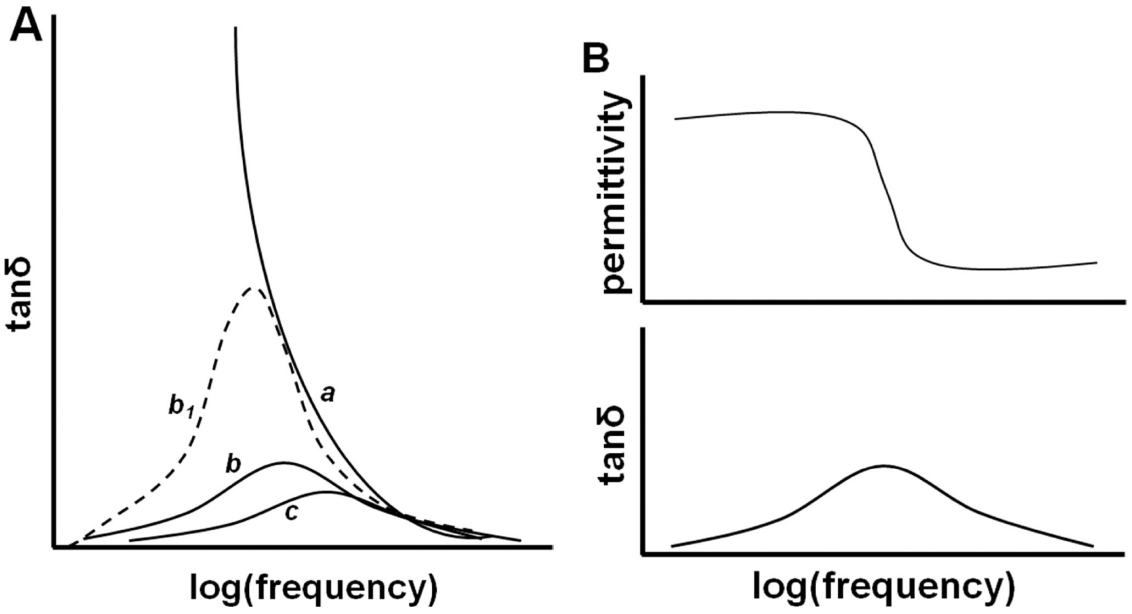

Figure 6. Wagner model predicted (A) loss angle tan δ for a composite with conducting phase of (a) pillars, (b) isolated spheres, (b_1) isolated randomly oriented ellipsoids, and (c) sheets, and (B) when tan δ peaks, the permittivity falls.

on the nanoparticle surfaces, the higher volume fraction nanocomposites should have greater surface areas, hence higher chain end densities, and hence greater contributions from reorientational polarization processes,[39] likely enhancing the relaxation processes observed at >3 GHz. Nevertheless, the 0.10 v_f Al-^{iso}PP nanocomposite is the most useful material for GHz range capacitor applications since the permittivity of ~6 is maintained above 5 GHz.

Modeling of Nanocomposite High Frequency Response. While the percolation theory has been employed to understand these types of conductive-insulating composites at low frequency, the mechanism of high frequency response has not been studied extensively; however, simple analytic mixing models can be employed to better understand the experimental frequency response of the present nanocomposites over a large frequency range. The nanocomposite capacitors of this study are composed of conducting regions (Al nanoparticles) and insulating regions (polypropylene matrix). Mixing theories, such as percolation theory,[20,21,55−64] developed for low frequency response suggest that at low volume fractions the individual particles act as completely isolated systems where the local field at the particle interface is similar to that at an interface between two isolated sheets. As the volume fraction of conducting filler first increases, the spherical particles first behave as isolated particles. Then, as the volume fraction continues to increase, some of the particles are sufficiently proximate to behave as a single extended dipole, that is, as "joint" particles with one dimension close to 2*d* (*d* is the average particle diameter) where the charges induced at the particle surfaces are now separated by the length of the aggregated particle cluster (compare Figure 2). Thus, the local polarization of these joint particles is larger than that of an isolated particle because the dipole moment ($p = qd$, where q is the amount of charge separated by distance, d) is larger. The density of these joint particles continues to increase with increasing particle volume fraction, and that increase also introduces joint particles of more complex shapes as well as the number of particles behaving jointly. Finally, when the percolation threshold is reached, there is a continuous path of particles from one electrode to the other, creating pillar-like structures. While trying to explain the frequency response, Wagner devised a simple model for the loss angle (tan δ) of dielectrics with conductive regions, useful when the conductive phase (here the filler) of the composite has either of three structures: sheets, isolated spheres, and pillars.[65,66] Wagner predicted that as the conductive phase morphology transitions from a sheet to spheres to pillars, the maximum in tan δ would shift to lower frequencies (Figure 6a). In 1937 Sillars[67] extended Wagner's simple model to include the response of ellipsoidal particles of conducting material (the transition between isolated spheres and pillars).

By this simple analysis, Sillars was able to explain the different tan δ shapes observed experimentally for filler particles of any dimensional axes *a*, *b*, and *c*.[67] This extension of Wagner's model is often called the MWS model (b_1 in Figure 6a results from this analysis). To evaluate composite dielectric loss quantitatively, Fricke[46,68] introduced a model of an inhomogeneous dielectric consisting of suspended homogeneous ellipsoids (axis $2a \geq 2b = 2c$), distributed randomly in a homogeneous medium. The complex conductivities eq 3, of the matrix and dispersed phases are, respectively, σ_1^* ($\sigma_{Al} \approx 3760$ S/m) and σ_2^* ($\sigma_{polypropylene} \approx 1.18 \times 10^{-17}$ S/m). In a low

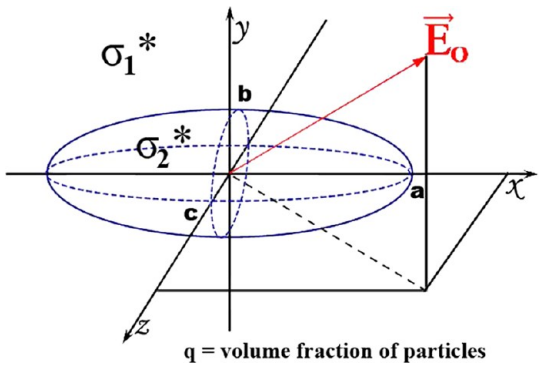

Figure 7. Representation of a nanoparticle of axes *a*, *b*, and *c* where $2a \geq 2b \geq 2c$ with an arbitrarily applied field E_o.

concentration suspension, the dispersed ellipsoids are assumed to be sufficiently far apart that the local field can be taken as equal to the external field.

$$\sigma^* = \sigma_1^* + \frac{1}{3} q(\sigma_2^* - \sigma_1^*) \sum_{j=a,b,c} \frac{(1+x_j)\sigma_1^*}{x_j\sigma_1^* + \sigma_2^*} \quad (3)$$

$$x_j = \frac{2 - abcL_j}{L_j} \quad (4)$$

$$L_j = \int_0^\infty \frac{ds}{(s+j^2)\sqrt{(s+a^2)(s+b^2)(s+c^2)}} \quad (5)$$

With the assumption that a mixture has an equal number of particles with the applied field aligned parallel to each of the three principal orientations, and if higher powers of q (the volume fraction) are neglected, the complex conductivity of the dispersion can be expressed as in eq 3, where q is the volume fraction of the dispersed ellipsoids and the x_j variables are shape factors depending on the ellipsoid axial ratios and their orientation with respect to the field (Figure 7). The values of x_j vary from zero for a flat oblate spheroid to infinity for a prolate spheroid. For cylinders arranged with their axes parallel to the electric field, $x = 1$. For spheres, $x = 2$, and eq 3 reduces to that given by Maxwell and Wagner.[69]

Separating σ^* into real and imaginary components, yields the complex permittivity[68] (eq 6, with A_σ, A_ε, B_σ, B_ε, and τ_j defined in eqs 7−11 where $\tau_1 = \varepsilon_o\varepsilon_1/\sigma_1$). The complex permittivity can then be separated into real and imaginary parts eqs 12, 13 and used to calculate tan δ for any composite structure. Here the metallic Al nanoparticle permittivity, ε, can be estimated using an extension of simple Drude theory.[65,70]

$$\varepsilon^* = \varepsilon_1 + \frac{\sigma_1}{i\omega\varepsilon_o} + \frac{\varepsilon_1}{3} q \sum_{j=a,b,c} (1+x_j) \frac{A_\sigma - B_\sigma + (\omega\tau_j)^2 A_\varepsilon}{1+(\omega\tau_j)^2} + \frac{\sigma_1}{3i\omega\varepsilon_o} q \sum_{j=a,b,c} (1+x_j) A_\sigma + \frac{i\omega\varepsilon_1}{3} q \sum_{j=a,b,c} (1+x_j)\tau_j \frac{A_\varepsilon + B_\sigma - A_\sigma}{1+(\omega\tau_j)^2} \quad (6)$$

$$A_\sigma = \frac{\sigma_2/\sigma_1 - 1}{\sigma_2/\sigma_1 + x_j} \quad (7)$$

$$A_\varepsilon = \frac{\varepsilon_2/\varepsilon_1 - 1}{\varepsilon_2/\varepsilon_1 + x_j} \quad (8)$$

$$B_\varepsilon = \frac{(1+x_j)\left(\frac{\sigma_2}{\sigma_1} - \frac{\varepsilon_2}{\varepsilon_1}\right)}{(\varepsilon_2/\varepsilon_1 + x_j)^2} \quad (9)$$

$$B_\sigma = \frac{(1+x_j)\left(\frac{\sigma_2}{\sigma_1} - \frac{\varepsilon_2}{\varepsilon_1}\right)}{(\sigma_2/\sigma_1 + x_j)^2} \quad (10)$$

$$\tau_j = \tau_1 \frac{\varepsilon_2/\varepsilon_1 + x_j}{\sigma_2/\sigma_1 + x_j} \quad (11)$$

$$\varepsilon' = \varepsilon_1 + \frac{\varepsilon_1}{3} q \sum_{j=a,b,c} (1+x_j) \frac{A_\sigma - B_\sigma + (\omega\tau_j)^2 A_\varepsilon}{1+(\omega\tau_j)^2} \quad (12)$$

$$\varepsilon'' = -\frac{\sigma_1}{\omega\varepsilon_o} - \frac{\sigma_1 q}{3\omega\varepsilon_o} \sum_{j=a,b,c} (1+x_j) A_\sigma + \frac{\omega\varepsilon_1}{3} q \sum_{j=a,b,c} (1+x_j)\tau_j \frac{A_\varepsilon + B_\sigma - A_\sigma}{1+(\omega\tau_j)^2} \quad (13)$$

Drude theory can be utilized to accurately describe bulk metal dielectric/optical properties,[70] but does not accurately describe the corresponding nanoparticle properties. The interband transition extension of Drude theory was developed to describe the interband electronic transitions observed in nanoparticles (that arise from confinement effects) and the large differences in local fields in and around the nanoparticle.[71] By fitting the optical properties of Al nanoparticles of various sizes to the interband model, coefficients that reproduce the frequency response of the permittivity are obtained.[71] Here, coefficients previously calculated in the literature[71] for 111.4 nm diameter nanoparticles are used, since the average diameter of the present Al nanoparticles is about 100 nm. From the real and imaginary parts of the permittivity calculated using eqs 12 and 13, the normalized tan δ can be calculated as $\varepsilon''/\varepsilon'$ (Figures 8 and 9), where the calculated tan δ values have been normalized to the highest calculated value for comparison among suggested structures.[66,72] By comparing peak positions in the plot for the normalized loss tangent as a function of the logarithmic frequency, the nature of the relaxation process and the relaxation frequency can be determined.[73] This normalization allows for easier comparison of the magnitudes of the tan δ calculated for each proposed structure.[72]

Here we utilize MWS modeling to understand how the expected joint particles will affect the frequency of the dielectric relaxation in these composites. Many

aggregate structural configurations are possible as the particle density increases. Explored here are two aggregation motifs: linear aggregation and planar aggregation, which essentially define prolate and oblate objects, respectively. In linear aggregation, spherical particles align along an axis to create a combined dipole, a joint particle as noted above, where the longest axial coefficient (2*a*) is equal to the number of particles connected times the average particle diameter, and the other two axes (2*b* and 2*c*) both equal the average particle diameter. If the field is aligned with the long axis of the particle the separation of charges on the joint particle surface (Figure 2) is a multiple of that of a single particle resulting in a larger MWS polarization response.

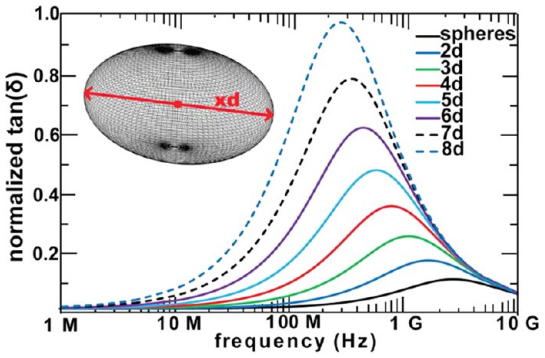

Figure 8. Computed dielectric loss (tan δ) response of Al nanocomposites containing randomly dispersed linear aggregates, where the aggregates are the length of multiple particles so that the long axis of the joint particle is 2*d*, 3*d*, *etc.*, where *d* is the average particle diameter and the nanoparticle volume fraction (*q*) is 0.02 Al.

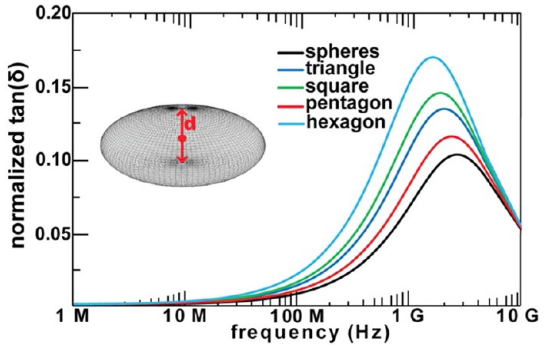

Figure 9. Computed dielectric loss (tan δ) response of Al nanocomposites composed of randomly dispersed planar aggregates as depicted in Scheme 2, where *d* is the average particle diameter, and with a volume fraction (*q*) of 0.02 Al.

As one of the many alternatives, the particles might also aggregate in planar structures. The simplest of these to model are triangular, square, etc. (Scheme 2). These planar aggregates have two axes (2*a* and 2*b*) defined by the diameter of the minimum circle inclosing the joint particles and one axis (2*c*, out of the plane of the page in Scheme 2) that is the average diameter of the particles. For these particles, when the shortest axis is perpendicular to the electrodes there is a large surface area for charge accumulation, leading to large MWS polarization. For both linear and planar aggregates, for a given volume fraction of Al, the relaxation frequency, or frequency at the maximum in tan δ, decreases as the number of nanoparticles in the joint particle increases (Figures 8 and 9).

MWS modeling predicts that as more joint particles of higher order (3 vs 2 particles) populate the film, the relaxation frequency will continue to fall. The predicted relaxation frequencies of 20−1000 MHz correspond well with the experimental relaxation data describing the dielectric permittivities of these composites, where most volume fractions undergo their first relaxation below 200 MHz. This model is useful not only to visualize dielectric relaxation in composites, but also to predict frequencies at which dielectric relaxation should occur. Percolation theory argues that at higher volume fractions, the nanoparticles should respond as joint particles, and MWS argues that these joint particles should lead to lower frequency dielectric relaxations which can be observed in the high frequency response of the nanocomposite permittivity (seen in Figures 4, 5, 8, and 9). Since these aggregate structures have more charge per structure that must reorganize over a larger geometry with the oscillating field, the response is slower and the surface polarization undergoes relaxation at lower frequencies than for a single, smaller particle. MWS equations provide an analytical form to estimate the magnitude of the correlation between particle size and relaxation frequency; the

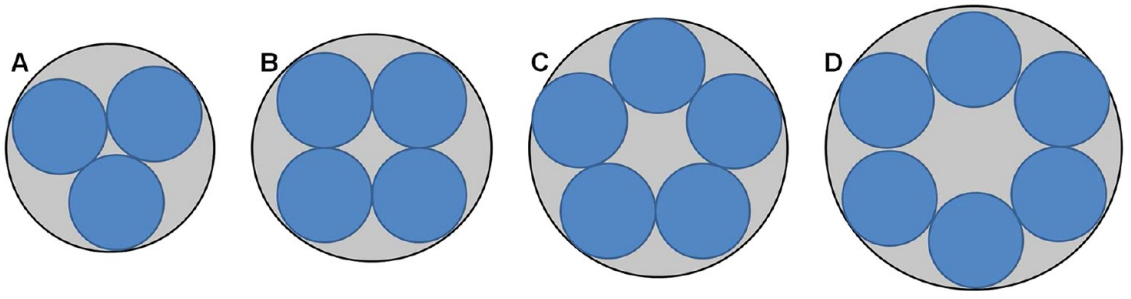

Scheme 2. Two-dimensional cartoon of possible planar nanoparticle aggregation motifs. The out-of-page axis is equal to one nanoparticle diameter.

larger the aggregate is, the greater is the charge that must be reorganized over a larger structure with every field oscillation, and thus the lower is the relaxation frequency.

It is interesting that the simplest prolate joint particles, that is, linear aggregates, are predicted to exhibit relaxation in the MHz range where all of the present nanocomposites appear to have their first relaxation. These aggregates have the largest total surface area per particle among the joint particles (*e.g.*, compared to oblate aggregates) leading to large linear internal surfaces on which charge can accumulate and polarize the interface. For the low volume fraction composites, this appears to be the only relaxation (Figures 4 and 5), whereas in the high volume fraction composites, there is a second GHz range relaxation which may indicate the presence of oblate joint particles. Oblate aggregates have the largest surface area on a single joint particle face and thus a large area on which accumulated charges can collectively respond to the oscillating field, resulting in large interfacial polarization. These observations are in agreement with percolation theoretical predictions that as the volume fraction of the conductive material increases, the number of joint particles and the complexity of the joint particles increases.[19−21,57,60,63,74,75] Thus, the composites with higher loadings should have higher aggregate nanoparticle densities, and the dielectric relaxation should shift to lower frequencies. Experimentally, this prediction is most clearly confirmed for the 0.124 volume fraction Al sample where a second relaxation is observed at ∼3 GHz (Figure 5), whereas the 0.104 Al composite has relatively constant permittivity up to 7 GHz (Figure 4).

CONCLUSIONS

In this study, a series of metallic Al nanoparticle−polypropylene dielectrics having relatively high permittivities are synthesized via *in situ* catalytic techniques, and the dielectric response is characterized over a broad frequency range as a function of nanoparticle volume fraction. Because the propylene polymerization takes place at organometallic catalyst centers anchored to these nanoparticles, the nanocomposites produced are randomly dispersed in the polyolefin matrix, with no visible structural defects that usually degrade film dielectric performance. The high conductivity of the Al nanoparticles leads to dielectric relaxations that can be described by MWS models, providing insight into how the nanoparticle volume fraction is correlated with the high frequency response. At higher Al nanoparticle volume fractions, the nanocomposites have greater densities of joint nanoparticles formed by aggregation that shift the dielectric relaxation to lower frequencies. Thus, the best performing capacitor in the series has a 0.104 Al volume fraction and a sustained permittivity of >6 for frequencies up to 7 GHz.

METHODS

Nanocomposite Synthesis. Al (d = 100 nm) nanoparticles with 2 nm native Al_2O_3 were purchased from Sigma-Aldrich. From the TEM it is clear that the particles range from about 50 nm to 150 nm in diameter. The nanoparticles were dried on a high vacuum line (10^{-5} Torr) at 80 °C overnight to remove the surface-bound water. The reagent [*rac*-ethylenebisindenyl]zirconium dichloride was purchased from Sigma-Aldrich and used as received. MAO, 10% solution in toluene, was also purchased from Sigma-Aldrich and was purified by removing the volatiles *in vacuo*. All manipulations of air-sensitive materials were performed with rigorous exclusion of O_2 and moisture using Schlenk techniques, or a high-vacuum line (10^{-6} Torr), or a N_2-filled MBraun glovebox with a high capacity recirculator (<1 ppm O_2 and H_2O). Propylene (Matheson, polymerization grade) was purified by passage through a supported MnO O_2-removal column and an activated Davison 4 A molecular sieve column. Toluene was dried using an activated alumina column and Q-5 columns, and was then vacuum-transferred from Na/K alloy and stored in Teflon-valve sealed bulbs.

In the glovebox, 2.0 g of nanoparticles, 200 mg of the metallocene precatalyst $EBIZrCl_2$ and 50 mL of toluene were loaded into a predried 200 mL flip-frit flask. The color of the particle suspension turned to light orange. The slurry mixture was subjected to alternating sonication and vigorous stirring overnight. The particles were then collected by filtration and washed with fresh toluene until the color of the toluene remained colorless. The particles were dried on the high-vacuum line overnight and stored in the glovebox at −40 °C in the dark.

In the glovebox, a 250 mL round-bottom three-neck Morton flask, equipped with a large magnetic stirring bar, was charged with 50 mL of dry toluene, 200 mg of the above catalyst-functionalized nanoparticles, and 50 mg of MAO. The assembled flask was removed from the glovebox, and the mixture was subjected to sonication and vigorous stirring for 30 min. The flask was then attached to a high vacuum line (10^{-5} Torr), the catalyst slurry was degassed, equilibrated at the desired reaction temperature using an external water bath, and saturated with 1.0 atm (pressure control using a mercury bubbler) of rigorously purified propylene while vigorously stirring. After a measured time interval (changing the interval results in different particle loadings), the polymerization was quenched by the addition of 5 mL of methanol, and the reaction mixture was then poured into 800 mL of methanol. The composite was allowed to fully precipitate overnight and was then collected by filtration, washed with fresh methanol, and dried on the high vacuum line at 80 °C overnight to constant weight.

Elemental analyses were performed by Midwest Microlabs, LLC, Indianapolis, Indiana. Inductively coupled plasma-optical emission spectroscopy (ICP-OES) analyses were performed by Galbraith Laboratories, Inc., Knoxville, Tennessee.

Film Fabrication. For this high frequency study, films with diameters between 3 and 7 mm are required. To obtain films that are robust to tearing at these diameters, relatively thick films were fabricated. The films were fabricated by slowly pressing the nanocomposite samples, that were heated slowly in a crucible until the composite powder was viscous (maximum surface temperature of crucible and composite was 100 °C), into the openings of small metal or PET washers, 3 mm in diameter and 1 mm thick. The thick films were then pressed with additional composite powder using a hot press at 100 °C and 500−800 psi pressure. The pressing helps create the smoothest electrode-dielectric interface possible. Postpressing vacuum

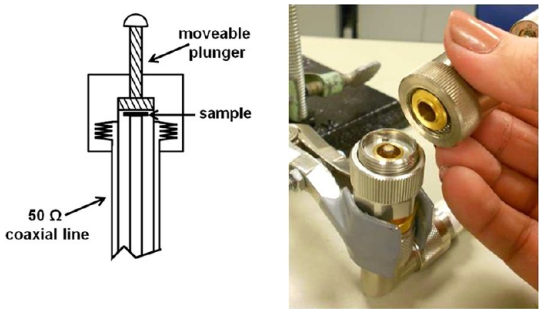

Scheme 3. Diagram and photograph of the "shorted coaxial cable" set up for high frequency lumped impedance measurements.

treatment at 80 °C was then performed overnight to remove any residual moisture and trapped air bubbles. Next, parallel-plate capacitors were fabricated by vapor-depositing gold electrodes on the dielectric nanocomposite films. Gold electrodes for metal−insulator−metal (MIM) devices were vacuum-deposited through shadow masks at (3−4) × 10^{-7} Torr (500 Å, 0.2−1.0 Å/s). The films were then removed from the washers by either cutting away the PET washer or boring the sample out of the metal washer.

Physical and Analytical Measurements. The thicknesses of the films were measured with calipers and used to calculate the dielectric permittivity and tan δ. Film topography and RMS roughnesses were imaged using a JEOL SPM atomic force microscope. The thick films had rms roughnesses of 3−4 nm. Low frequency (1 MHz) capacitance was measured on an HP 4384A precision meter. High frequency loss was measured using a lumped impedance method, described below.

Lumped Impedance Measurements. High frequency capacitance was measured using a lumped impedance method on an HP 8510 network analyzer whose sample holder terminated in an APC7 connector. This connector was fitted with the "shorted coaxial cable" sample holder as shown in Scheme 3. Each 3 mm thick film sample was placed directly on the center of the APC7 and then enclosed in the sample holder. The sample holder was fitted with an electrode at the end of a movable plunger which is brought into contact with the upper film surface by tightening the feed screw. In this configuration the sample holder inductance is minimized. To measure the high frequency capacitance, a lumped impedance method of measuring the complex reflection coefficient (both magnitude, Γ, and phase, θ) is utilized. By placing a thick sample (~1 mm) at the end of the coaxial line, the reflection coefficient of the impedance transported down the line can be measured. Before measuring an unknown capacitor, a calibration was performed by attaching known standards (short, open, and load) to the end of the coaxial line.

Conflict of Interest: The authors declare no competing financial interest.

Acknowledgment. This research was supported by ONR (MURI N00014-05-1-0766; dielectric science) and by DOE (DE-FG02-86ER13511; surface polymerization catalysis). The project made use of Central Facilities supported by the NSF MRSEC program (DMR-1121262) at the Materials Research Center of Northwestern U. We thank J. Long, S. Perini, and the equipment staff at Penn State U. for assistance with the high frequency equipment.

REFERENCES AND NOTES

1. Dang, Z. M.; Wu, J. B.; Fan, L. Z.; Nan, C. W. Dielectric Behavior of Li and Ti Co-Doped NiO/PVDF Composites. *Chem. Phys. Lett.* **2003**, *376*, 389–394.
2. Dang, Z.-M.; Lin, Y.-H.; Nan, C.-W. Novel Ferroelectric Polymer Composites with High Dielectric Constants. *Adv. Mater.* **2003**, *15*, 1625–1629.
3. Michalczyk, P.; Bramoulle, M. Ultimate Properties of the Polypropylene Film for Energy Storage Capacitors. *IEEE Trans. Magn.* **2003**, *39*, 362–365.
4. Rabuffi, M.; Picci, G. Status Quo and Future Prospects for Metallized Polypropylene Energy Storage Capacitors. *IEEE Trans. Plasma Sci.* **2002**, *30*, 1939–1942.
5. Gross, S.; Camozzo, D.; Di Noto, V.; Armelao, L.; Tondello, E. PMMA: A Key Macromolecular Component for Dielectric Low-K Hybrid Inorganic−Organic Polymer Films. *Eur. Polym. J.* **2007**, *43*, 673–696.
6. Kim, P.; Doss, N. M.; Tillotson, J. P.; Hotchkiss, P. J.; Pan, M.-J.; Marder, S. R.; Li, J.; Calame, J. P.; Perry, J. W. High Energy Density Nanocomposites Based on Surface-Modified $BaTiO_3$ and a Ferroelectric Polymer. *ACS Nano* **2009**, *3*, 2581–2592.
7. Li, J.; Claude, J.; Norena-Franco, L. E.; Seok, S. I.; Wang, Q. Electrical Energy Storage in Ferroelectric Polymer Nanocomposites Containing Surface-Functionalized $BaTiO_3$ Nanoparticles. *Chem. Mater.* **2008**, *20*, 6304–6306.
8. Li, J.; Seok, S. I.; Chu, B.; Dogan, F.; Zhang, Q.; Wang, Q. Nanocomposites of Ferroelectric Polymers with TiO_2 Nanoparticles Exhibiting Significantly Enhanced Electrical Energy Density. *Adv. Mater.* **2009**, *21*, 217–221.
9. Tanaka, T.; Montanari, G. C.; Mülhaupt, R. Polymer Nanocomposites as Dielectrics and Electrical Insulation—Perspectives for Processing Technologies, Material Characterization and Future Applications. *IEEE Trans. Dielectr. Electr. Insul.* **2004**, *11*, 763–784.
10. Bai, Y.; Cheng, Z. Y.; Bharti, V.; Xu, H. S.; Zhang, Q. M. High-Dielectric-Constant Ceramic−Powder Polymer Composites. *Appl. Phys. Lett.* **2000**, *76*, 3804–3806.
11. Qi, L.; Lee, B. I.; Chen, S.; Samuels, W. D.; Exarhos, G. J. High-Dielectric-Constant Silver−Epoxy Composites as Embedded Dielectrics. *Adv. Mater.* **2005**, *17*, 1777–1781.
12. Ogihara, H.; Randall, C. A.; Trolier-McKinstry, S. High-Energy Density Capacitors Utilizing 0.7 $BaTiO_3$−0.3 $BiScO_3$ Ceramics. *J. Am. Ceram. Soc.* **2009**, *92*, 1719–1724.
13. Wang, Y.; Zhou, X.; Chen, Q.; Chu, B.; Zhang, Q. Recent Development of High Energy Density Polymers for Dielectric Capacitors. *IEEE Trans. Dielectr. Electr. Insul.* **2010**, *17*, 1036–1042.
14. Tomer, V.; Manias, E.; Randall, C. A. High Field Properties and Energy Storage in Nanocomposite Dielectrics of Poly(vinylidene fluoride−hexafluoropropylene). *J. Appl. Phys.* **2011**, *110*, 044107.
15. Xia, W.; Xu, Z.; Wen, F.; Zhang, Z. Electrical Energy Density and Dielectric Properties of Poly(vinylidene fluoride−chlorotrifluoroethylene)/$BaSrTiO_3$ Nanocomposites. *Ceram. Int.* **2012**, *38*, 1071–1075.
16. Fredin, L. A.; Li, Z.; Lanagan, M. T.; Ratner, M. A.; Marks Tobin, J. Enhanced Energy Storage and Suppressed Dielectric Loss in Oxide Core−Shell Polyolefin Nanocomposites by Moderating Internal Surface Area and Increasing Shell Thickness. *Adv. Mater.* **2012**, 10.1002/adma.201202183.
17. Shen, Y.; Lin, Y.; Li, M.; Nan, C.-W. High Dielectric Performance of Polymer Composite Films Induced by a Percolating Interparticle Barrier Layer. *Adv. Mater.* **2007**, *19*, 1418–1422.
18. George, S.; Sebastian, M. T. Three-Phase Polymer−Ceramic−Metal Composite for Embedded Capacitor Applications. *Compos. Sci. Technol.* **2009**, *69*, 1298–1302.
19. Gonon, P.; Boudefel, A. Electrical Properties of Epoxy/Silver Nanocomposites. *J. Appl. Phys.* **2006**, *99*, 024308/1–024308/8.
20. Grannan, D. M.; Garland, J. C.; Tanner, D. B. Critical Behavior of the Dielectric Constant of a Random Composite near the Percolation Threshold. *Phys. Rev. Lett.* **1981**, *46*, 375–8.
21. Yang, R.; Wong, C. P. Ultra High Dielectric Constant Epoxy Silver Composite for Embedded Capacitor Application. *Proc. Electron. Compon. Technol. Conf.* **2002**, 920–923.
22. Panda, M.; Srinivas, V.; Thakur, A. K. On the Question of Percolation Threshold in Polyvinylidene Fluoride/Nanocrystalline Nickel Composites. *Appl. Phys. Lett.* **2008**, *92*, 132905–3.

23. Panda, M.; Srinivas, V.; Thakur, A. K. Surface and Interfacial Effect of Filler Particle on Electrical Properties of Polyvinyledene Fluoride/Nickel Composites. *Appl. Phys. Lett.* **2008**, *93*, 242908–3.
24. Williams, L. A.; Marks, T. J. Synthesis, Characterization, and Heterogeneous Catalytic Implementation of Sulfated Alumina Nanoparticles. Arene Hydrogenation and Olefin Polymerization Properties of Supported Organozirconium Complexes. *ACS Catal.* **2011**, *1*, 238–245.
25. Wegener, S. L.; Marks, T. J.; Stair, P. C. Design Strategies for the Molecular Level Synthesis of Supported Catalysts. *Acc. Chem. Res.* **2011**, *45*, 206–214.
26. Nicholas, C. P.; Marks, T. J. Sulfated Tin Oxide Nanoparticles as Supports for Molecule-Based Olefin Polymerization Catalysts. *Nano Lett.* **2004**, *4*, 1557–1559.
27. Williams, L. A.; Guo, N.; Motta, A.; Delferro, M.; Fragalà, I. L.; Miller, J. T.; Marks, T. J. Surface Structural-Chemical Characterization of a Single-Site d0 Heterogeneous Arene Hydrogenation Catalyst Having 100% Active Sites. *Proc. Natl. Acad. Sci. U.S.A.* **2012**, DOI: PNAS201220240.
28. Li, Z.; Fredin, L. A.; Tewari, P.; DiBenedetto, S. A.; Lanagan, M. T.; Ratner, M. A.; Marks, T. J. *In Situ* Catalytic Encapsulation of Core−Shell Nanoparticles Having Variable Shell Thickness: Dielectric and Energy Storage Properties of High-Permittivity Metal Oxide Nanocomposites. *Chem. Mater.* **2010**, *22*, 5154–5164.
29. Guo, N.; DiBenedetto, S. A.; Kwon, D.-K.; Wang, L.; Russell, M. T.; Lanagan, M. T.; Facchetti, A.; Marks, T. J. Supported Metallocene Catalysis for *in Situ* Synthesis of High Energy Density Metal Oxide Nanocomposites. *J. Am. Chem. Soc.* **2007**, *129*, 766–767.
30. Guo, N.; DiBenedetto, S. A.; Tewari, P.; Lanagan, M. T.; Ratner, M. A.; Marks, T. J. Nanoparticle, Size, Shape, and Interfacial Effects on Leakage Current Density, Permittivity, and Break Down Strength of Metal Oxide−Polyolefin Nanocomposites: Experiment and Theory. *Chem. Mater.* **2010**, *22*, 1567–1578.
31. Fredin, L. A.; Li, Z.; Lanagan, M. T.; Ratner, M. A.; Marks, T. J. Substantial Recoverable Energy Storage in Percolative Metallic Aluminum−Polypropylene Nanocomposites. *Adv. Funct. Mater.* **2012**, in press.
32. TRAK Ceramics, I., Dielectric Materials. In *Overview & Application Notes*; Group, N. M., Ed.; TRAK Ceramics, Inc.: Hagerstown, MD, 2012.
33. Ho, C.-Y.; Chang, C.-C.; Lee, J.-Y. High-Frequency Dielectric Characterization for Liquid Crystalline Polyimide/SiO_2 Nanocomposites. *J. Appl. Polym. Sci.* **2010**, *117*, 3454–3459.
34. Zhou, W.; Yu, D. Effect of Coupling Agents on the Dielectric Properties of Aluminum Particles Reinforced Epoxy Resin Composites. *J. Compos. Mater.* **2011**, *45*, 1981–1989.
35. Zhang, Y.; Wang, Y.; Deng, Y.; Li, M.; Bai, J. Enhanced Dielectric Properties of Ferroelectric Polymer Composites Induced by Metal−Semiconductor Zn−ZnO Core−Shell Structure. *ACS Appl. Mater. Interfaces* **2012**, *4*, 65–68.
36. Baker-Jarvis, J.; Janezic, M.; Degroot, D. High-Frequency Dielectric Measurements. *IEEE Instrum. Meas. Mag.* **2010**, *13*, 24–31.
37. Advances in High-Frequency PCB Materials. *Defense Tech. Briefs* **2010**, *4*, 4-7.
38. Dimos, D.; Mueller, C. H. Perovskite Thin Films for High-Frequency Capacitor Applicaitons. *Annu. Rev. Mater. Sci.* **1998**, *28*, 397–419.
39. Kremer, F.; Schönhals, A. *Broadband Dielectric Spectroscopy*; Springer: New York, 2003.
40. Ku, C. C.; Liepins, R. *Electrical Properties of Polymers*; Hanser: München, 1987.
41. Jonscher, A. K. *Dielectric Relaxation in Solids*; Chelsea Dielectric Press: London, 1983.
42. Feldman, Y.; Puzenko, A., Ryabov, Y., Dielectric Relaxation Phenomena in Complex Materials. In *Fractals, Diffusion and Relaxation in Disordered Complex Systems: A Special Vol. of Advances in Chemical Physics*; Coffey, W. T., Kalmykov, Y. P., Rice, S. A., Eds.; John Wiley & Sons: New York, 2006; Vol. 133, Part A.
43. Blinov, L. M. *Electro-Optical and Magneto-Optical Properties of Liquid Crystals*. Wiley: Chichester, 1983.
44. Asami, K. Characterization of Heterogeneous Systems by Dielectric Spectroscopy. *Prog. Polym. Sci.* **2002**, *27*, 1617–1659.
45. Popielarz, R.; Chiang, C. K.; Nozaki, R.; Obrzut, J. Dielectric Properties of Polymer/Ferroelectric Ceramic Composites from 100 Hz to 10 GHz. *Macromolecules* **2001**, *34*, 5910–5915.
46. Fricke, H. A Mathematical Treatment of the Electric Conductivity and Capacity of Disperse Systems I. The Electric Conductivity of a Suspension of Homogeneous Spheroids. *Phys. Rev.* **1924**, *24*, 575–587.
47. Von Hippel, A. R. *Dielectric Materials and Applications*; MIT Press: Cambridge, MA, 1966.
48. Stuchly, S. S.; Rzepecka, M. A.; Iskander, M. F. Permittivity Measurements at Microwave Frequencies Using Lumped Elements. *IEEE Trans. Instrum. Meas.* **1974**, *23*, 56–62.
49. Stuchly, S. S.; Matuszewski, M. A Combined Total Reflection-Transmission Method in Application to Dielectric Spectroscopy. *IEEE Trans. Instrum. Meas.* **1978**, *27*, 285–288.
50. Atwater, H. A. *Introduction to Microwave Theory*; McGraw-Hill: Tokyo, 1962.
51. Bordi, F.; Cametti, C.; Motta, A. Scaling Behavior of the High-Frequency Dielectric Properties of Poly-L-lysine Aqueous Solutions. *Macromolecules* **2000**, *33*, 1910–1916.
52. Kofod, G.; Risse, S.; Stoyanov, H.; McCarthy, D. N.; Sokolov, S.; Kraehnert, R. Broad-Spectrum Enhancement of Polymer Composite Dielectric Constant at Ultralow Volume Fractions of Silica-Supported Copper Nanoparticles. *ACS Nano* **2011**, *5*, 1623–1629.
53. Nies, C. W., Deyneka, E., Lanagan, M. T. In *Measurement of Dielectric Properties of $BaTiO_3$-Based Materials in the 10 MHz to 1 GHz Frequency Range*, Proceedings of the Tenth US−Japan Seminar on Dielectric and Piezoelectric Ceramics, Providence Biltmore, Providence, Rhode Island, Sept 26−29, 2001.
54. Smyth, C. P. Dielectric Polarization and Relaxation. *Annu. Rev. Phys. Chem.* **1966**, *17*, 433–456.
55. Brosseau, C.; Beroual, A.; Boudida, A. How Do Shape Anisotropy and Spatial Orientation of the Constituents Affect the Permittivity of Dielectric Heterostructures? *J. Appl. Phys.* **2000**, *88*, 7278–7288.
56. Dang, Z. M.; Fan, L. Z.; Shen, Y.; Nan, C. W. Study on Dielectric Behavior of a Three-Phase Cf/(PVDF + $BaTiO_3$) Composite. *Chem. Phys. Lett.* **2003**, *369*, 95–100.
57. Fisch, R.; Harris, A. B. Critical Behavior of Random Resistor Networks near the Percolation Threshold. *Phys. Rev. B* **1978**, *18*, 416.
58. Gelves, G. A.; Lin, B.; Sundararaj, U.; Haber, J. A. Low Electrical Percolation Threshold of Silver and Copper Nanowires in Polystyrene Composites. *Adv. Funct. Mater.* **2006**, *16*, 2423–2430.
59. Gascoin, N.; Gillard, P.; Baudry, G. Characterisation of Oxidised Aluminium Powder: Validation of a New Anodic Oxidation Bench. *J. Hazard. Mater.* **2009**, *171*, 348–357.
60. Nan, C. Physics of Inhomogeneous Inorganic Materials. *Prog. Mater. Sci.* **1993**, *37*, 1–116.
61. Pham Thi, M.; Velasco, G.; Colomban, P. Percolation Threshold and Interface Optimization in a Hup/C Double-Layer Supercapacitor. *J. Mater. Sci. Lett.* **1986**, *5*, 415–17.
62. Scher, H.; Zallen, R. Critical Density in Percolation Processes. *J. Chem. Phys.* **1970**, *53*, 3759–3761.
63. Xu, J.; Wong, C. P. Low-Loss Percolative Dielectric Composite. *Appl. Phys. Lett.* **2005**, *87*, 082907/1–082907/3.
64. Zhou, K.; Boggs, S. A.; Ramprasad, R.; Aindow, M.; Erkey, C.; Alpay, S. P. Dielectric Response and Tunability of a Dielectric−Paraelectric Composite. *Appl. Phys. Lett.* **2008**, *93*, 102908.
65. Ashcroft, N. W.; Mermin, N. D. *Solid State Physics*; Saunders: Philadelphia, PA: 1976.
66. Wagner, K. W. Dielektrische Eigenschaften Von Verschiedenen Isolierstoffen. *Electron. Eng. (Arch. Elektrotech.)* **1914**, *3*, 67–106.
67. Sillars, R. W. The Properties of a Dielectric Containing Semiconducting Particles of Various Shapes. *J. Inst. Electron. Eng.* **1937**, *80*, 378–394.

68. Fricke, H. The Maxwell–Wagner Dispersion in a Suspension of Ellipsoids. *J. Phys. Chem.* **1953**, *57*, 934–937.
69. Wang, Q.; Zhu, L. Polymer Nanocomposites for Electrical Energy Storage. *J. Polym. Sci., Part B: Polym. Phys.* **2011**, *49*, 1421–1429.
70. Ordal, M. A.; Bell, R. J.; Alexander, J. R. W.; Long, L. L.; Querry, M. R. Optical Properties of Fourteen Metals in the Infrared and Far Infrared: Al, Co, Cu, Au, Fe, Pb, Mo, Ni, Pd, Pt, Ag, Ti, V, and W. *Appl. Opt.* **1985**, *24*, 4493–4499.
71. Peng, Y.; Wang, Y.; Yang, Y.; Dlott, D. Simulation of the Absorption Spectra of Nanometallic Al Particles with Core–Shell Structure: Size-Dependent Interband Transitions. *J. Nanopart. Res.* **2010**, *12*, 777–787.
72. Maxwell, J. C.; Thompson, J. J. *A Treatise on Electricity and Magnetism*; Clarendon: Oxford, 1892.
73. Leyva, M. E.; Barra, G. M. O.; Moreira, A. C. F.; Soares, B. G.; Khastgir, D. Electric, Dielectric, and Dynamic Mechanical Behavior of Carbon Black/Styrene-Butadiene-Styrene Composites. *J. Polym. Sci., Part B: Polym. Phys.* **2003**, *41*, 2983–2997.
74. Jylhä, L.; Sihvola, A. Equation for the Effective Permittivity of Particle-Filled Composites for Material Design Applications. *J. Phys. D: Appl. Phys.* **2007**, *40*, 4966.
75. Toker, D.; Azulay, D.; Shimoni, N.; Balberg, I.; Millo, O. Tunneling and Percolation in Metal–Insulator Composite Materials. *Phys. Rev. B* **2003**, *68*, 041403.